

## J-Groove에 의한 환형 제트 펌프 캐비테이션 성능 개선

최영도\*<sup>†</sup> · 쉬레스트 우즈왈\*\*

### Cavitation Performance Improvement of an Annular Jet Pump by J-Groove

Young-Do Choi\*<sup>†</sup>, Ujjwal Shrestha\*\*

*Key Words* : Annular jet pump (환형제트펌프), J-Groove (J-그루브), Cavitation Performance (캐비테이션 성능), Pressure coefficient (압력 계수), Vapor Volume Fraction (증기 체적 분율)

#### ABSTRACT

Jet pump contributes to transport sensitive objects of liquid single phase flow or solid-liquid two-phase flow, which has a merit of very simple structure without moving body. However, the pump has a inevitable demerit of cavitation occurrence in the pump passage and the cavitation phenomenon damages the transport object. This paper presents the numerical investigation to improve the cavitation performance of an annular jet pump (AJP) using J-Groove. J-Groove is the passive rectangular grooves installed on the wall of pump mixing zone passage to the flow direction and the grooves entrain high pressure fluid from the diffuser to the throat of AJP. The installation of J-Groove on the pump passage wall increases the pressure in the mixing zone of AJP and improves the pump cavitation performance. In this study, the effectiveness of J-Groove has been evaluated by the parametric study of J-Groove design variables (depth, length, angle and number). The study results reveal that each design variable of J-Groove has its influence on the increase of fluid pressure in the mixing zone of AJP.

#### 1. Introduction

The jet pump is a type of pump used to transfer energy from primary fluid flow to secondary flow by the Venturi effect. Jet pumps are simple in design and manufacturing. Unlike centrifugal and reciprocating pumps, the jet pump does not have any moving components. The absence of moving components eradicates the friction loss, rotor-stator interaction, and other operational problems associated with lubrication, bearing, and sealing<sup>(1)</sup>. The main disadvantage of the jet pump is low efficiency ranging to 40% and low pumping height<sup>(2)</sup>.

The main components of the jet pump are the

primary pipe, secondary pipe, nozzle, diffuser, and outlet pipe. The working mechanism of the jet pump is to convert the pressure energy from the primary fluid into the velocity energy through a nozzle. The high-pressure fluid moves through the primary pipe. When the primary flow passes through the nozzle, it increases the fluid velocity and generates the low-pressure zone in the throat, which withdraws secondary flow via the secondary pipe. Eventually, primary flow and secondary flow mixed in the throat, and the velocity energy converts back into pressure energy.

According to the shape, the jet pump is classified into two types: central jet pump (CJP) and annular jet

\* Department of Mechanical Engineering, Institute of New and Renewable Energy Technology Research, Mokpo National University

\*\* Graduate School, Department of Mechanical Engineering, Mokpo National University

† 교신저자, E-mail : ydchoi@mokpo.ac.kr

pump (AJP)<sup>(3)</sup>. The central jet pump (CJP) is the most commonly used. The CJP applies the primary fluid to the inner nozzle and secondary fluid flow through a surrounding annular nozzle. The AJP is another type of jet pump. In the AJP, the primary fluid flows through an annular nozzle and the secondary fluid flows through the central nozzle. Therefore, the AJP is most suited for the hydraulic transport of large and delicate solids such as potatoes, fish, shellfish, etc.

For the CJPs, there are numerous studies related to geometrical design and operational parameters<sup>(4-6)</sup>. On the other hand, there are few studies related to the AJPs. Shimizu et al.<sup>(7)</sup> have experimented on different configurations of AJP. They concluded that the maximum efficiency of AJP is 36%, depending on the configuration. Elger et al.<sup>(3)</sup> showed that the recirculation flow occurs at the center of the mixing section in the AJP. Hammoud<sup>(8)</sup> explained the effect of the nozzle-to-throat spacing to nozzle diameter on the jet pump performance. Kwon et al.<sup>(9)</sup> conducted a numerical analysis in the AJP. He explained that there is an occurrence of recirculation and reverse flow in the AJP at a low mass ratio<sup>(9)</sup>. Song et al.<sup>(10)</sup> showed that the AJP transports liquid and solid particles efficiently. When mass ratio increases to the critical value, the inception of cavitation will occur. The cavitation causes serious injury to the body of fish<sup>(11)</sup>. The cavitation in the AJP occurs when the pressure falls below the vapor pressure.

Among the methods of anti-cavitation occurrence, J-Groove is selected for the improvement of cavitation

performance of the AJP. This paper investigates the parametric study of J-Groove design variables. The main purpose of this work is to demonstrate the effectiveness of J-Groove on the improvement of cavitation performance in the AJP.

## 2. Test Pump and Methodology

### 2.1 Test pump

Fig. 1 shows the schematic view and nomenclature of an annular jet pump (AJP) model. The test pump model of AJP has been adopted from the previous studies<sup>(12-13)</sup>. The main components of the AJP are primary inlet, secondary inlet, nozzle, throat, diffuser and outlet. The most significant parameter for the AJP is the convergence and divergence angle. Moreover, the diameter and length of the throat are crucial for the proper mixing of primary and secondary flow. The range of the relative throat length is 2.17–2.89 times the throat diameter<sup>(12)</sup>.

The main design parameters of the annular jet pump are primary inlet diameter ( $D_p$ ), secondary inlet diameter ( $D_s$ ), throat diameter ( $D_t$ ), outlet diameter ( $D_d$ ), diffuser length ( $L_d$ ), convergence angle ( $\alpha$ ) and divergence angle ( $\beta$ ). The dimension of AJP design parameters are  $D_p = 100$  mm,  $D_s = 80$  mm,  $D_t = 60$  mm,  $D_d = 125$  mm,  $L_d = 500$  mm,  $\alpha = 20^\circ$  and  $\beta = 7^\circ$ . The AJP can be identified by the area ratio,  $m$ . The area ratio,  $m$  is calculated as indicated in Eq. (1), and fixed to  $m = 1.75$  in this study.

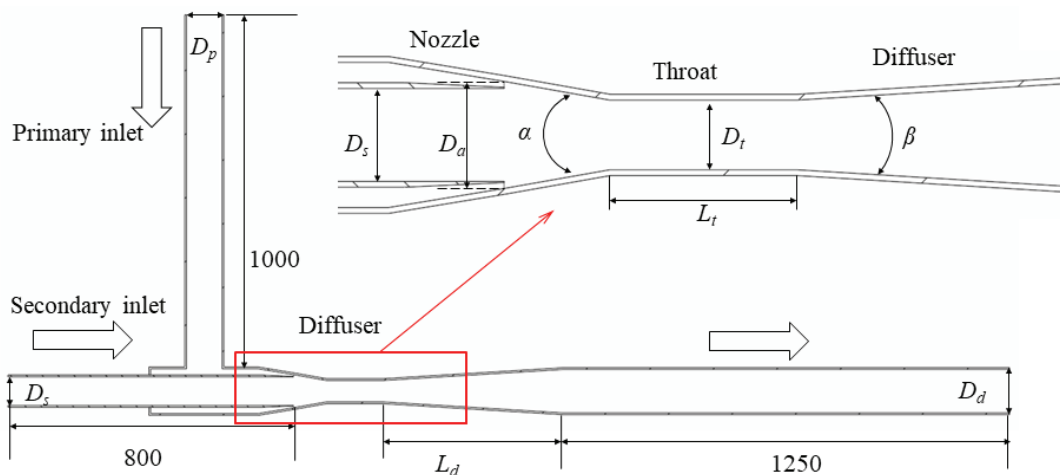


Fig. 1 Schematic view of an annular jet pump (AJP) model

$$m = \frac{A_t}{A_j} \quad (1)$$

$$A_j = \frac{\pi}{4} (D_a^2 - D_s^2) \quad (2)$$

$$A_t = \frac{\pi}{4} D_t^2 \quad (3)$$

where  $m$  is area ratio,  $A_j$  is cross section area of annular jet,  $A_t$  is cross section area of throat,  $D_a$  diameter of annular ring,  $D_s$  is diameter of secondary pipe,  $D_t$  is diameter of throat.

## 2.2 Design of J-Groove for AJP

The previous study suggested that the AJP is prone to the recirculation flow<sup>(3)</sup> and cavitation at the throat region<sup>(11)</sup>. The J-Groove is the passive method for the suppression of the swirl flow and cavitation. The installation of the J-Groove has successfully suppressed the swirl flow and cavitation in inducer<sup>(14)</sup>, Francis turbine<sup>(15)</sup>, and pump-turbine<sup>(16)</sup>.

Fig. 2 shows the schematic view of J-Groove mechanism of reverse jet flow inducement in the groove passages. J-Groove is the rectangular groove passages installed on the wall of diffuser to the flow direction. J-Groove entrains the reverse flow from the high pressure to low pressure regions in the groove passages. And the reverse jet flow, which has relatively higher pressure, mixes with the main flow, which has relatively lower pressure, at the upstream edge of the groove. Therefore, the reverse jet flow increases the pressure of main stream at the throat and diffuser sections of the AJP.

The design of J-Groove for the AJP is shown in Fig. 3. The main design parameters for the J-Groove are length ( $l$ ), depth ( $d$ ), angle ( $\theta$ ) and number ( $n$ ). In the AJP, the mixing zone is divided into the nozzle, throat, and diffuser sections. Therefore, the length of J-Groove in the AJP is categorized as  $l_1$ ,  $l_2$ , and  $l_3$ . The main objective of J-Groove installation is to direct the high pressurized fluid from the diffuser towards the throat through the groove passages in the AJP.

In this study, various types of J-Groove specification

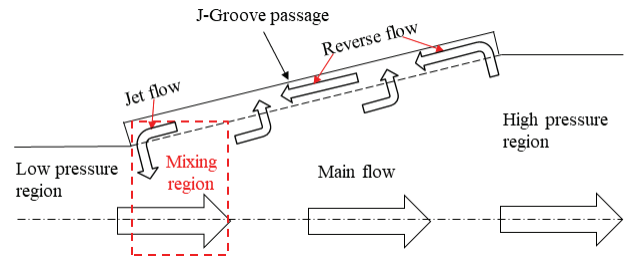


Fig. 2 Schematic view of J-Groove mechanism in diffuser

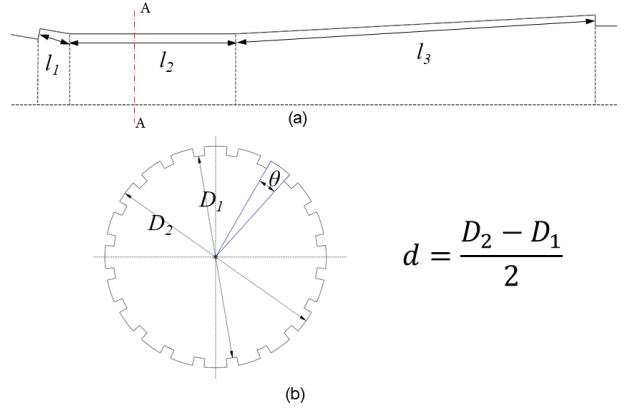


Fig. 3 Design parameters of J-Groove in the AJP mixing zone: (a) Front view (b) cross sectional view

are evaluated for the cavitation performance improvement under the fixed condition of pump specification as explained in the previous chapter.

## 2.3 Numerical Methodology

The CFD analysis was used to investigate the flow behavior in the AJP in detail. CFD analysis was conducted by using a commercial code of ANSYS-CFX 19.2<sup>(17)</sup>. The flow in the jet pump has been assumed as steady and incompressible states because the flow field in AJP is simple and without any moving bodies. The previous studies also suggested that incompressible steady state is better for the CFD analysis of AJP<sup>(1,8,12,13)</sup>. The realizable  $\kappa$ - $\epsilon$  model has been used for computational analysis<sup>(13)</sup>. The realizable  $\kappa$ - $\epsilon$  model uses variable turbulent viscosity. It derives transport equation for dissipation rate from mean-square vorticity fluctuation. As a result it gives improved predictions for the spreading of the jets<sup>(18)</sup>. The realizable  $\kappa$ - $\epsilon$  model can treat the viscous sub-layer near the wall, when  $y^+$  value is less than 5<sup>(17)</sup>. Therefore, in this study  $y^+$  value for each components

Table 1 Boundary conditions for the CFD analysis of the AJP

Parameter/Boundary	Value/Conditions
Primary inlet	Total pressure
Secondary inlet	Mass flow rate
Outlet	Static pressure
Turbulence model	Realizable $k-\varepsilon$ turbulence model
Wall	No slip condition

is less than 5 to predict the viscous sub-layer.

The numerical grid in the flow field domain for the AJP is shown in Fig. 4. The numerical grids in Fig. 4 represent the mixing zone of the AJP. The structured hexahedral grids have been generated by ANSYS ICEM 19.2<sup>(17)</sup> for the computational analysis. The cross section of J-Groove is indicated in Fig. 4.

The inlet boundary conditions were total pressure and mass flow rate for primary and secondary inlets, respectively. The outlet boundary condition was static pressure. The detailed boundary conditions for CFD analysis of AJP are shown in Table 1. The mass ratio ( $q$ ), pressure ratio ( $p$ ), and efficiency ( $\eta$ ) were used to evaluate the performance of AJP, which are calculated by using Eqs. (4), (5), and (6), respectively<sup>(19)</sup>.

$$q = \frac{Q_s}{Q_n} \quad (4)$$

$$p = \frac{p_m^T - p_s^T}{p_n^T - p_m^T} \quad (5)$$

$$\eta = p \times q \quad (6)$$

where  $q$  is mass ratio,  $p$  is pressure ratio,  $\eta$  is efficiency,  $Q_s$  is secondary flow rate,  $Q_n$  is flow rate at nozzle exit,  $p_m^T$  is total pressure at diffuser outlet,  $p_s^T$  is total pressure at secondary inlet,  $p_n^T$  is total pressure at nozzle exit.

The cavitation phenomenon in the AJP is observed by using a homogeneous mixture of water and water vapor at 25°C. The Rayleigh-Plesset equation is used to predict the cavitation occurrence in this study.

The selection of the proper numerical grid is critical for the CFD analysis. Therefore, a mesh dependency

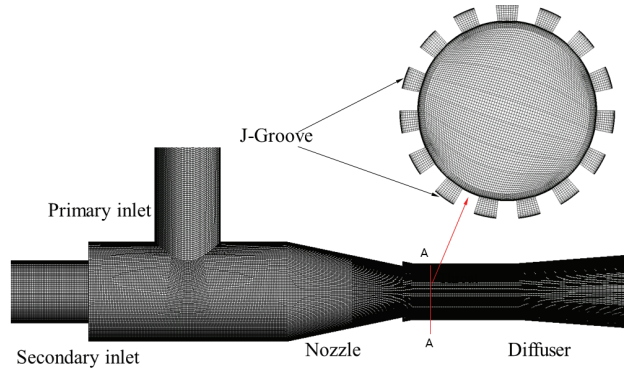


Fig. 4 Numerical grid of the AJP for CFD analysis

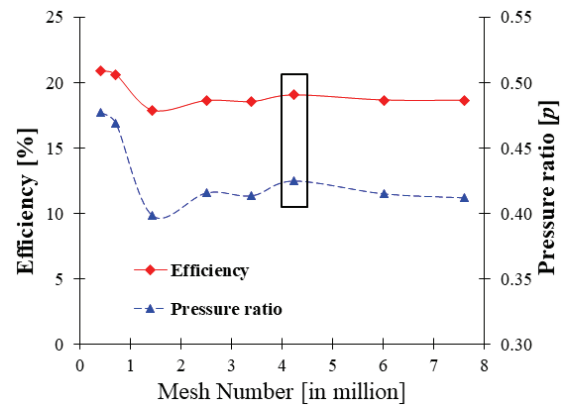


Fig. 5 Mesh dependency test for the AJP CFD analysis at  $q=0.45$

test was conducted to evaluate the effect of numerical grids on CFD analysis results. Fig. 5 shows the results of the mesh dependency test. Finally, the numerical grids with 4.2 million nodes are selected for further analysis. The  $y^+$  value for numerical grids of the primary inlet, secondary inlet, nozzle, diffuser and outlet are 3.54, 0.33, 2.75, 0.73, and 0.14, respectively.

The detailed information of the numerical grid is indicated in Table 2.

Table 2 Information of numerical grids for the AJP

Components	Node number	$y^+$ value
Primary inlet	631000	3.54
Secondary inlet	491904	0.33
Nozzle	801600	2.75
Diffuser	935940	0.73
Outlet	1369200	0.14
<b>Total</b>	<b>4229644</b>	

### 3. Results and Discussion

#### 3.1 Test pump performance and validation

The experimental and reference CFD analysis data from Long et al.<sup>(13)</sup> has been used to validate the CFD analysis results of present study. The performance of the AJP from experiment and CFD analysis were compared as shown in Fig. 6. The results indicate that the comparison between experimental and CFD analysis results shows a sound agreement in the pressure ratio and efficiency with the variation of mass ratio of AJP.

#### 3.2. Internal flow behavior

The internal flow of the AJP has been investigated with various mass ratios. When the AJP operates at the lower mass ratio, there is a significant amount of recirculation flow at the nozzle section of the AJP. The recirculation flow at the nozzle section can be decreased with an increase in the mass ratio. As indicated in Fig. 7, the recirculation flow has been suppressed with an increase in the mass ratio. When  $q=0.8$ , there is no recirculation flow in the mixing section. Fig. 8 indicates the measuring location in the AJP. The  $x/D_t = 0$  indicates the outlet of secondary pipe in the AJP.

The dynamic pressure is used to evaluate the mixture of high velocity primary flow and secondary flow. The dynamic pressure is estimated by Eq. 7.

$$C_v = 0.5\rho U^2 \quad (7)$$

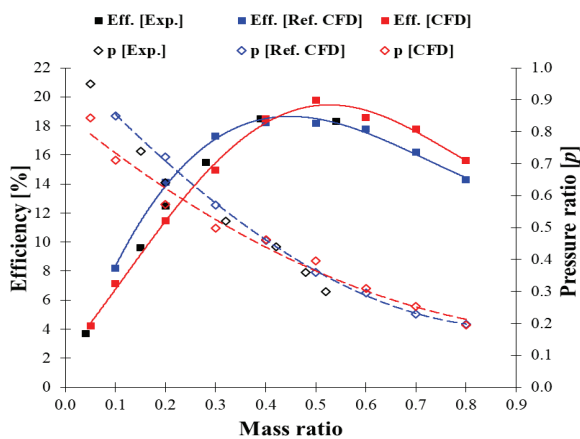


Fig. 6 Validation of CFD analysis results with Long et al.<sup>(13)</sup> at  $m=1.75$

where  $C_v$  is dynamic pressure,  $\rho$  is density of water at 25°C,  $U$  is velocity at central line of the AJP.

Fig. 9 indicates the dynamic pressure distribution in the AJP. The dynamic pressure in the mixing zone for the mass ratio of  $q=0.8$  is comparatively higher than the case of  $q=0.1$ . Moreover, when the mass ratio is relatively higher, the secondary flow has higher dynamic pressure in the secondary inlet pipe passage. The results imply that the higher dynamic pressure contributes to the proper mixture between the primary and secondary flows in the throat section of the AJP.

#### 3.3 Pressure distribution

The pressure coefficient is used to calculate and investigate the pressure distribution in the centerline

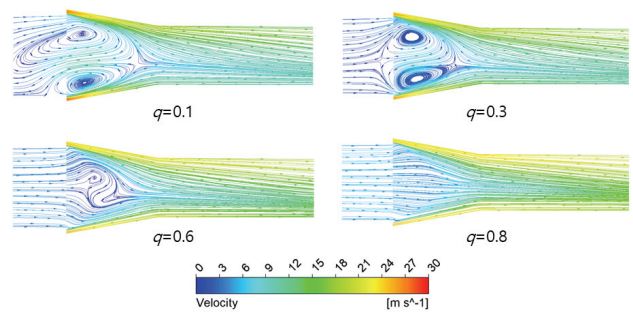


Fig. 7 Velocity streamlines distribution in the AJP at different mass ratio

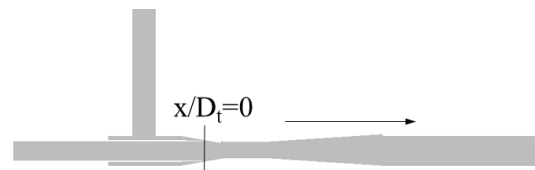


Fig. 8 Measuring location in the central line of the AJP

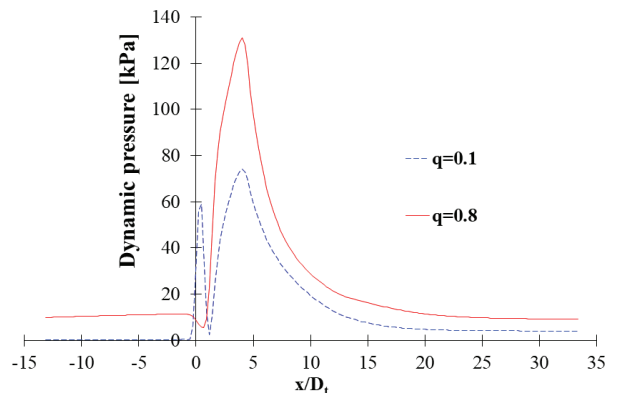


Fig. 9 Dynamic pressure distribution in the AJP

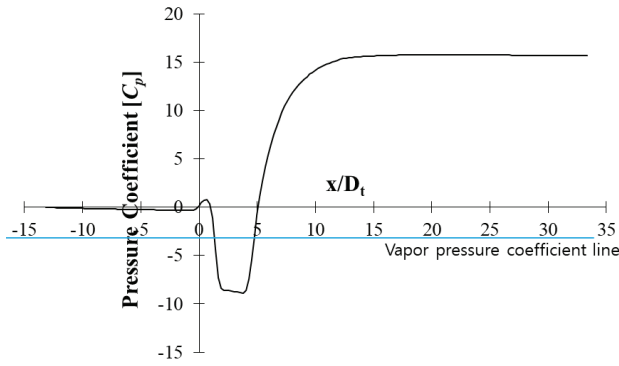


Fig. 10 Pressure coefficient distribution in the AJP at  $q=0.8$  of the AJP. The pressure coefficient is calculated by using Eq. 8<sup>(20)</sup>.

$$C_p = \frac{p_x - p_s}{0.5\rho U_p^2} \quad (8)$$

where  $C_p$  is pressure coefficient,  $p_x$  is static pressure at central line of the AJP,  $p_s$  is static pressure at secondary inlet,  $U_p$  is velocity at primary inlet.

The pressure coefficient distribution at  $q=0.8$  is shown in Fig. 10. The pressure coefficient at the throat region is below the vapor pressure coefficient. The vapor pressure coefficient is calculated by substituting saturated vapor pressure ( $p_v$ ) in the place of  $p_x$ .

When the pressure coefficient value is below the vapor pressure coefficient line, it concerns the occurrence of cavitation inception in that region, Fig. 10 suggests the possibility of cavitation in the throat of the AJP at  $q=0.8$ .

The cavitation may cause serious damage and injuries to sensitive objects. Therefore, the pressure coefficient distribution should be improved and increased above the vapor pressure line for the safe transportation of the sensitive objects.

### 3.4 Effect of J-Groove shape

The main aim of the J-Groove installation in the mixing zone of the AJP is to transfer the high pressure fluid from the diffuser to the jet nozzle and throat sections. Therefore, the various shape design of J-Groove has been implemented in the AJP to evaluate the pressure coefficient distribution. The effect of

J-Groove has been examined at  $q=0.8$ .

#### 3.4.1 Effect of J-Groove depth ( $d$ )

The depth of J-Groove is one of the significant design parameters. The influence of depth on the increase of pressure coefficient in the mixing zone of the AJP is discussed in this section. Table 3 shows the variety of the depth in the design of J-Groove. The depth of J-Groove is varied from 1.5 mm to 6 mm and the depths are calculated by the equation shown in Fig. 3b). Fig. 11 illustrates the effect of the J-Groove depth on the improvement of the pressure coefficient at the mixing zone of the AJP. The results imply that the depth of J-Groove plays a significant role in the

Table 3 Design variables for J-Groove with various depth ( $d$ )

Length ( $l_1$ )	19 mm	19 mm				
Length ( $l_2$ )	162 mm	162 mm				
Length ( $l_3$ )	501 mm	501 mm				
Angle ( $\theta$ )	12°	12°	12°	12°	12°	12°
Number ( $n$ )	15	15	15	15	15	15
<b>Depth (<math>d</math>)</b>	<b>1.5 mm</b>	<b>2.5 mm</b>	<b>3.5 mm</b>	<b>4.5 mm</b>	<b>5.5 mm</b>	<b>6 mm</b>

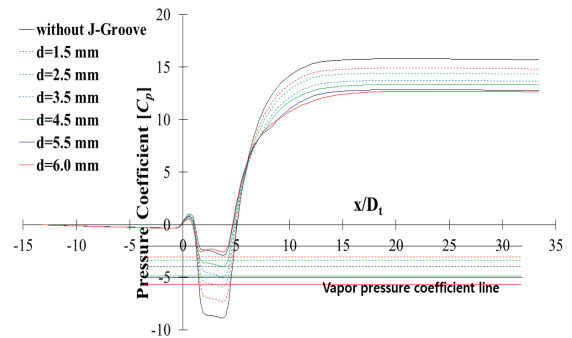


Fig. 11 Variation of pressure coefficient in the AJP with various J-Groove depth ( $q=0.8$ )

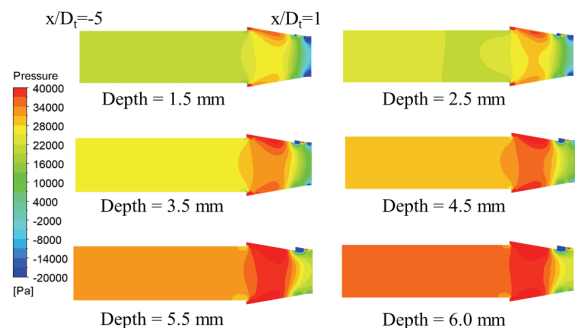


Fig. 12 Pressure distribution in the AJP with various J-Groove depth ( $d$ ) at  $x/D_t$  from -5 to 1 ( $q=0.8$ )

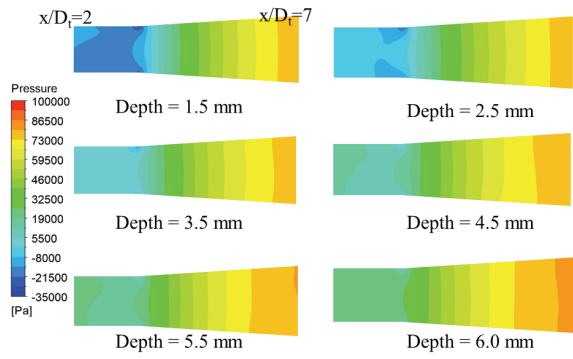


Fig. 13 Pressure distribution in the AJP with various J-Groove depth ( $d$ ) at  $x/D_t$  from 2 to 7 ( $q=0.8$ )

increase of pressure distribution in the mixing zone.

In order to visualize the pressure increase according to the J-Groove depth, the two different locations are selected as shown in Figs. 12 and 13. Fig. 12 shows the pressure contours in the AJP at  $-5 \leq x/D_t \leq 1$ . The pressure is increasing at the secondary pipe passage with an increase of the J-Groove depth. Similarly, Fig. 13 shows the pressure contours in the AJP at  $2 \leq x/D_t \leq 7$ . The increase of depth increases the passage pressure in the mixing zone of the AJP.

Table 4 shows the variation of the vapor pressure coefficient in the AJP according to the J-Groove depth, which is resulted from the secondary inlet pressure variation as shown in Fig. 12.

Fig. 14 shows the velocity vectors with reverse flow along the J-Groove passage. It clarifies that the installation of the J-Groove on the diffuser wall induces the reverse flow. Stronger reverse flow is visible at  $d=5.5$  mm compared to that at  $d=1.5$  mm. Therefore, the depth of J-Groove is directly related to the strength of reverse flow in J-Groove. The high intensity reverse flow helps to increase the pressure at the mixing zone of the AJP. Thus, the deeper J-Groove is efficient to increase pressure at the mixing zone.

### 3.4.2 Effect of J-Groove length ( $l_j$ )

The different J-Groove lengths ( $l_j$ ) from 5 mm to 20 mm are shown in Table 5 and the effect of J-Groove length on the increase of pressure coefficient is shown in Fig. 15. The variation of pressure coefficient distribution indicates that the J-Groove length  $l_j$  has a significant influence on the improvement of pressure coefficient at the mixing zone of the AJP. The extension of  $l_j$  helps to improve the pressure coefficient at the

Table 4 Variation of vapor pressure coefficient with J-Groove depth ( $d$ )

Different depth ( $d$ )	Vapor pressure coefficient
Without J-Groove	-2.18048
1.5 mm	-3.61121
2.5 mm	-3.84975
3.5 mm	-4.77971
4.5 mm	-5.62339
5.5 mm	-5.74857
6.0 mm	-6.58589

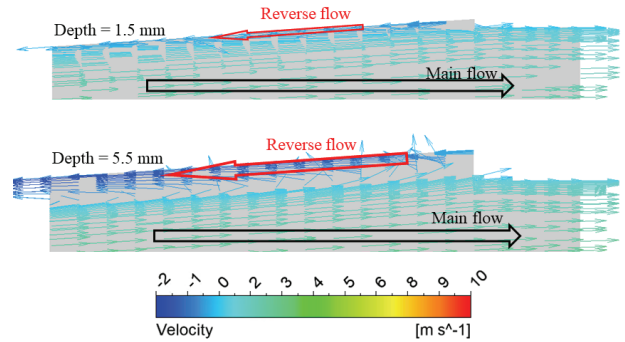


Fig. 14 Velocity vectors with reverse flow in J-Groove passage at  $q=0.8$

Table 5 Design variables for J-Groove with various length ( $l_j$ )

Length ( $l_j$ )	5 mm	7.5 mm	10 mm	12.5 mm	15 mm	20 mm
Length ( $l_2$ )	162 mm	162 mm	162 mm	162 mm	162 mm	162 mm
Length ( $l_3$ )	501 mm	501 mm	501 mm	501 mm	501 mm	501 mm
Angle ( $\theta$ )	12°	12°	12°	12°	12°	12°
Number ( $n$ )	15	15	15	15	15	15
Depth ( $d$ )	6 mm	6 mm	6 mm	6 mm	6 mm	6 mm

throat section of the AJP. Therefore, it is obvious that the effect of the length ( $l_j$ ) has an essential role in the improvement of pressure coefficient at the mixing zone of the AJP.

### 3.4.3 Effect of J-Groove angle ( $\theta$ )

The J-Groove angle ( $\theta$ ) helps to predict the width of the J-Groove. Table 6 shows the design variables for J-Groove with various angles.

Fig. 16 shows the effect of the J-Groove angle on the pressure coefficient distribution. The wider J-Groove shape improves the higher pressure coefficient distribution. However, the increase of the pressure coefficient according to the J-Groove width is limited below the vapor pressure coefficient lines, which

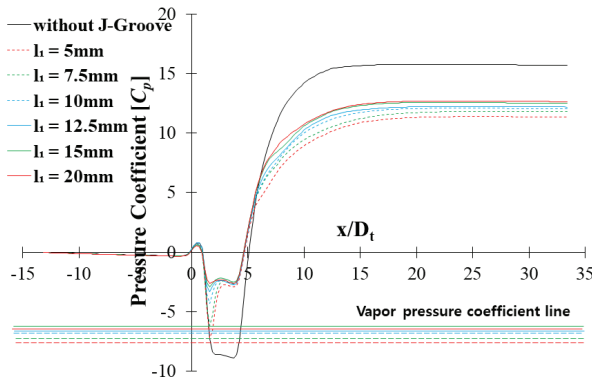


Fig. 15 Pressure coefficient distribution with various J-Groove length ( $l_i$ ) ( $q=0.8$ )

Table 6 Design variables for J-Groove with various angle ( $\theta$ )

Length ( $l_1$ )	19 mm					
Length ( $l_2$ )	162 mm					
Length ( $l_3$ )	501 mm					
Angle ( $\theta$ )	8°	10°	12°	14°	16°	18°
Number ( $n$ )	15	15	15	15	15	15
Depth ( $d$ )	2.5 mm					

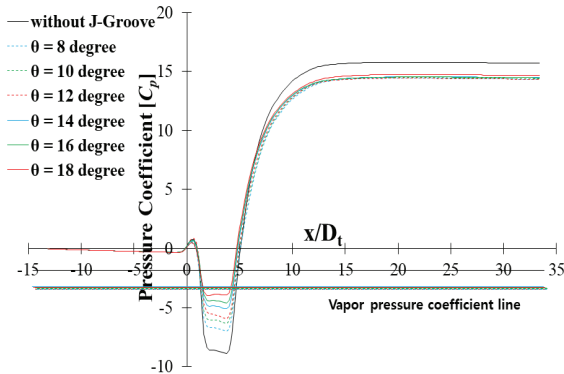


Fig. 16 Pressure coefficient distribution with various J-Groove angle ( $\theta$ ) ( $q=0.8$ )

reveals that the effectiveness of the J-Groove width is relatively low.

### 3.4.4 Effect of J-Groove number ( $n$ )

J-Groove number specifically affects the surface area covered by J-Groove. The variation of J-Groove design with J-Groove number ( $n$ ) is shown in Table 7. Fig. 17 indicates the improvement in the pressure coefficient distribution in the AJP by J-Groove number. The increase in the J-Groove number has a positive but limited effect on the pressure coefficient

distribution. The results indicate that the effectiveness of J-Groove directly depends on the surface area covered by J-Groove in the mixing zone.

### 3.5 Effect on the pump performance

The effect of J-Groove installation on the pump performance is investigated. Table 8 indicates J-Groove design specification for the examination and Fig. 18 shows the comparison between the cases without and with J-Groove for the performance of the AJP.

The efficiency in the case with J-Groove installation shows 2% decrease at the best efficiency point in comparison with that without J-Groove. It is clear that the decrease of efficiency is originated from the

Table 7 Design variables for J-Groove with various number ( $n$ )

Length ( $l_1$ )	19 mm				
Length ( $l_2$ )	162 mm				
Length ( $l_3$ )	501 mm				
Angle ( $\theta$ )	12°	12°	12°	12°	12°
Number ( $n$ )	10	12	15	18	20
Depth ( $d$ )	2.5 mm				

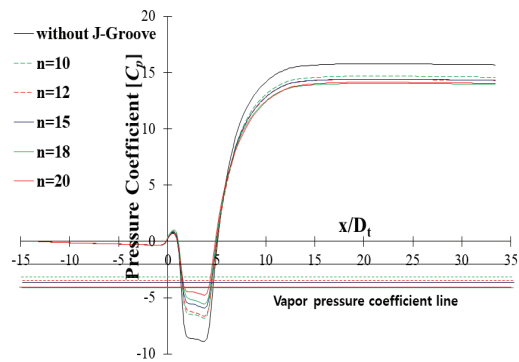


Fig. 17 Pressure coefficient distribution with various J-Groove number ( $n$ ) ( $q=0.8$ )

Table 8 J-Groove design specification for pump performance comparison

J-Groove parameters	Value
Length ( $l_1$ )	19 mm
Angle ( $\theta$ )	12°
Number ( $n$ )	15
Depth ( $d$ )	5.5 mm

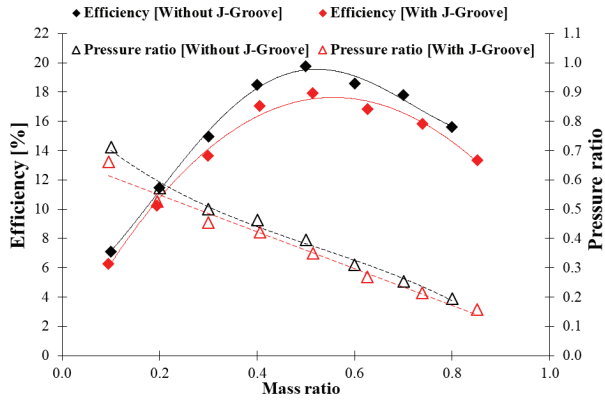


Fig. 18 Comparison of pump performance without and with J-Groove

decrease of pressure ratio in the case with J-Groove as indicated in Fig. 18.

Therefore, in order to increase the pump efficiency in the case with J-Groove installation, more careful and suitable selection of J-Groove shape based on the increase of pressure at the mixing zone as well as the suppression of pressure decrease at the pump outlet is required.

### 3.6 Improvement of Cavitation Performance

The cavitation analysis has been performed in the AJP with different cavitation numbers. The nozzle cavitation number and effective head for the AJP is defined in Eqs. 9<sup>(21)</sup> and 10.

$$\sigma_n = \frac{p_n - p_v}{0.5\rho v_n^2} \quad (9)$$

$$H = \frac{p_o^t - p_s^t}{\rho g} \quad (10)$$

where  $\sigma_n$  is nozzle cavitation number,  $p_n$  is static pressure at the exit of nozzle,  $p_v$  is saturated vapor pressure,  $p_o^t$  is total pressure at the pump outlet,  $p_s^t$  is total pressure at the secondary inlet,  $v_n$  is velocity at the outlet of nozzle,  $H$  is effective head of the AJP,  $\rho$  is water density at 25°C,  $g$  is acceleration due to gravity.

The cavitation performance without and with J-Groove has been compared at the mass ratio of

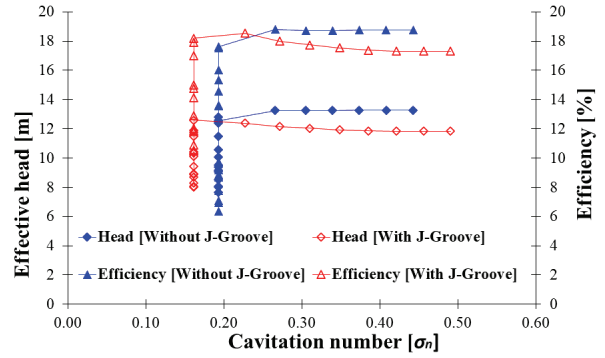


Fig. 19 Comparison of cavitation performance without and with J-Groove in the AJP at  $q=0.4$

$q=0.4$ . Fig. 19 clearly indicates the improvement of cavitation performance by J-Groove installation, which includes more extension to the lower nozzle cavitation number for the pump efficiency and effective head. The nozzle cavitation number has been decreased from 0.195 to 0.162 with installation of J-Groove. Therefore, J-Groove helps to operate the AJP at lower nozzle cavitation number. Figs. 20 and 21 show the comparison of vapor volume fraction in the cases without and with J-Groove installation. The value 0 of vapor volume fraction indicates the state of water only, but 1.0 means the state of water vapor (cavitation inception) only. The installation of J-Groove has significantly reduced the vapor volume fraction in the AJP from 0.63 to 0.08 at  $q=0.4$  and static pressure at pump outlet,  $p_o=70$  kPa.

The vapor volume fraction distribution at  $q=0.8$  has been shown in Fig. 22. When  $q=0.8$ , the installation of J-Groove decrease the vapor volume fraction from 0.77 to 0.38 at  $p_o=80$  kPa and 0.70 to 0.11 at  $p_o=90$

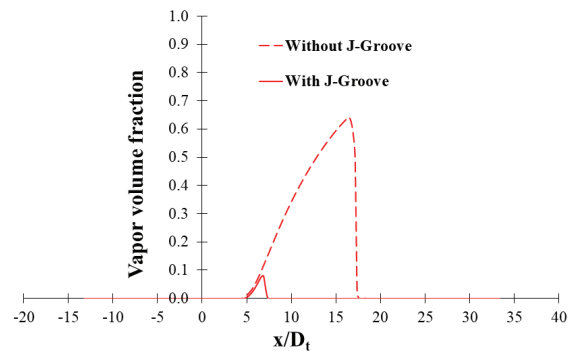


Fig. 20 Comparison of vapor volume fraction without and with J-Groove in the AJP at  $q=0.4$  and  $p_o=70$ kPa

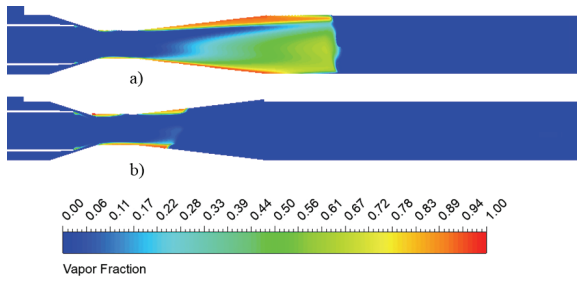


Fig. 21 Comparison of vapor volume fraction contours a) without and b) with J-Groove in the AJP at  $q=0.4$  and  $p_o=70\text{kPa}$

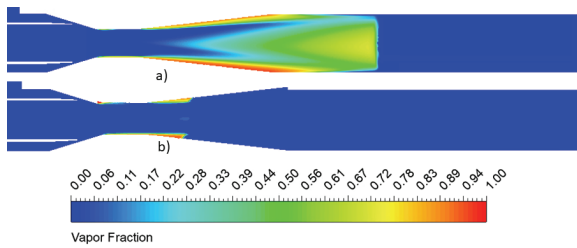


Fig. 23 Comparison of vapor volume fraction contours a) without and b) with J-Groove in the AJP at  $q=0.8$  and  $p_o=90\text{ kPa}$

kPa respectively. The area under the vapor volume fraction has been reduced drastically. Figs. 23 and 24 explain more clearly that the vapor volume fraction has been decreased significantly with the installation of J-Groove. The installation of the J-Groove suppresses the cavitation occurrence efficiently. Thus, it leads the AJP to transport sensitive objects with less damage.

#### 4. Conclusions

In this study, the vulnerability of current design of AJP to the cavitation has been indicated. The optimization of the current design of AJP might not able to improve the cavitation performance. Therefore, the application of J-Groove in the annular jet pump (AJP) has been carried out. While installing J-Groove, various design parameters of J-groove (length, depth, angle and number) have been studied. By conducting CFD analysis, the effects of J-Groove design parameters have been evaluated. Each design parameter has their influence on the improvement of pressure distribution in the mixing zone of the AJP.

J-Groove depth ( $d$ ) makes a significant improvement

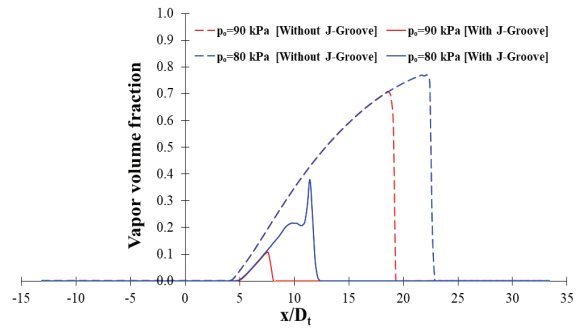


Fig. 22 Comparison of vapor volume fraction without and with J-Groove in the AJP at  $q=0.8$

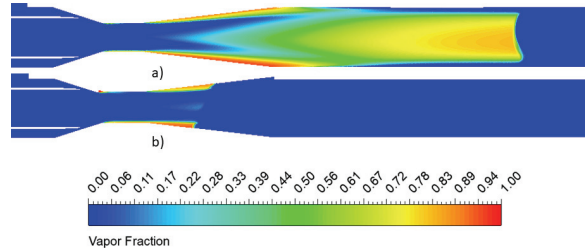


Fig. 24 Comparison of vapor volume fraction contours a) without and b) with J-Groove in the AJP at  $q=0.8$  and  $p_o=80\text{ kPa}$

in the pressure distribution in the mixing zone of the AJP. The deeper J-Groove passage achieves the higher pressure distribution in the AJP. J-Groove length ( $l$ ) shows the effect on the pressure distribution largely at the inlet of the throat. Similarly, the effectiveness of width and angle of J-Groove passage surely exists, but is limited to some extents.

Consequently, J-Groove is effective on the improvement of the pressure distribution in the pump mixing zone and the increased fluid pressure in the pump can suppress the cavitation occurrence significantly. Therefore, the AJP with J-Groove installation can transport sensitive objects without any serious damage by cavitation.

However, despite the improvement in cavitation performance by the installation of J-Groove, the degraded pump efficiency should be recovered by the optimal selection of J-Groove parameters.

#### Acknowledgement

This research (work) was supported by the long-term overseas training program of Mokpo National University in 2019.

## References

- (1) Deng, X., Dong, J., Wang, Z. and Tu, J., 2017, "Numerical analysis of an annular water-air jet pump with self-induced oscillation mixing chamber," *The Journal of Computational Multiphase Flows*, Vol. 9, No. 1, pp. 47-53.
- (2) Lisowski, E. and Momeni, H., 2010, "CFD modelling of a jet pump with circumferential nozzles for large flow rates," *Archives of Foundry Engineering*, Vol. 10, No. Special issue 3, pp. 69-72.
- (3) Elger, D. F., Taylor, S. J. and Liou, C. P., 1994, "Recirculation in an annular-type jet pump," *Journal of Fluids Engineering*, Vol. 116, pp. 735-740.
- (4) Hatzlavramidis, D. T., 1991, "Modeling and design of jet pumps," *SPE Production Engineering*, pp. 413-419.
- (5) Narabayashi, T., Yamazaki, Y., Kobayashi, H. and Shakouchi, T., 2006, "Flow analysis for single and multi-nozzle jet pump," *JMSE International Journal*, Vol. 49, No. 4, pp. 933-940.
- (6) Zhu, H., Qiu, B., Jia, Q. and Yang, X., 2011, "Simulation analysis of hydraulic jet pump," *Advanced Materials Research*, Vol. 204-210, pp. 293-296.
- (7) Shimizu, Y., Nakamura, S., Kuzuhara S. and Kurata, S., 1987, "Studies of the configuration and performance of annular type jet pumps," *Journal of Fluids Engineering*, Vol. 190, pp. 205-212.
- (8) Hammoud, A. H., 2006, "Effect of design and operational parameters on jet pump performance," in *Proceedings of the 4th WSEAS International Conference on Fluid Mechanics and Aerodynamics*, Elounda, Greece.
- (9) Kwon, O. B., Kim, M. K., Kwon, H. C. and Bae, D. S., 2002, "Two-dimensional numerical simulations on the performance of an annular jet pump," *Journal of Visualization*, Vol. 5, No. 1, pp. 21-28.
- (10) Song, X. G., Park, J. H., Kim, S. G. and Park, Y. C., 2013, "Performance comparison and erosion prediction of jet pumps by using a numerical method," *Mathematical and Computer Modelling*, Vol. 57, pp. 245-253.
- (11) Xiao, L., Long, X., Li, L., Xu, M., Wu, N. and Wang, Q., 2015, "Movement characteristics of fish in a jet fish pump," *Ocean Engineering*, Vol. 108, pp. 480-492.
- (12) Long, X. P., Zeng, Q. L., Yang, X. L. and Xiao, L., 2012, "Structure optimization of an annular jet pump using design of experiment method and CFD," *IOP Conf. Series: Earth and Environmental Science*, Vol. 15, p. 7.
- (13) Long, X., Xu, M., Lyu, Q. and Zhu, J., 2016, "Impact of the internal flow in a jet fish pump on the fish," *Ocean Engineering*, vol. 126, pp. 313-320.
- (14) Choi, Y-D., Junichi, K. and Imamura, H., 2007, "Suppression of cavitation in inducers by J-Grooves," *Journal of Fluids Engineering*, Vol. 129, pp. 15-22.
- (15) Chen, Z. and Choi, Y-D., 2018, "Suppression of cavitation in the draft tube of Francis turbine model by J-Groove," *Journal of Mechanical Science*, Vol. 233, No. 9, pp. 3100-3110.
- (16) Shrestha, U., Singh, P. M. and Choi, Y-D., 2019, "Suppression of flow instability in draft tube of pump turbine using J-Groove," *Korean Society of Fluid Machinery*, Vol. 22, No. 6, pp. 5-13.
- (17) ANSYS Inc., "ANSYS Customer Portal," [Online]. <https://support.ansys.com/AnsysCustomerPortal>. [Accessed 10 January 2018].
- (18) Shih, T. H., Liou, W. W., Shabbir, A., Yang, Z. and Zhu, J., 1995, "A new k-ε eddy viscosity model for high reynolds number turbulent flows," *Computers Fluids*, Vol. 24, No. 3, pp. 227-238.
- (19) Elger, D. F., Mclam, E. T. and Taylor, S. J., 1991, "A new way to represent jet pump performance," *Journal of Fluids Engineering*, Vol. 113, pp. 439-444.
- (20) Guo, M. and Choi, Y-D., 2020, "Flow passage shape design of a high pressure multistage centrifugal pump for performance improvement and miniaturization," *Korean Society of Fluid Machinery*, Vol. 23, No. 2, pp. 42-50.
- (21) Guo, M. and Choi, Y-D., 2020, "Effect of impeller blade thickness on the performance and internal flow characteristics of a single channel pump model," *Korean Society of Fluid Machinery*, Vol. 23, No. 1, pp. 15-22.